

Role of Solvation Dynamics in Excited State Proton Transfer of 1-Naphthol in Nanoscopic Water Clusters Formed in a Hydrophobic Solvent

Surajit Rakshit, Ranajay Saha, Pramod Kumar Verma and Samir Kumar Pal*

Unit for Nano Science and Technology, Department of Chemical, Biological and Macromolecular Sciences, S. N. Bose National Centre for Basic Sciences, Salt Lake, Kolkata, India

Received 22 January 2012, accepted 7 March 2012, DOI: 10.1111/j.1751-1097.2012.01140.x

ABSTRACT

Excited state proton transfer (ESPT) in biologically relevant organic molecules in aqueous environments following photoexcitation is very crucial as the reorganization of polar solvents (solvation) in the locally excited (LE) state of the organic molecule plays an important role in the overall rate of the ESPT process. A clear evolution of the two photoinduced dynamics in a model ESPT probe 1-naphthol (NpOH) upon ultrafast photoexcitation is the motive of the present study. Herein, the detailed kinetics of the ESPT reaction of NpOH in water clusters formed in hydrophobic solvent are investigated. Distinct values of time constants associated with proton transfer and solvent relaxation have been achieved through picosecond-resolved fluorescence measurements. We have also used a model solvation probe Coumarin 500 (C500) to investigate the dynamics of solvation in the same environmental condition. The temperature dependent picosecond-resolved measurement of ESPT of NpOH and the dynamics of solvation from C500 identify the magnitude of intermolecular hydrogen bonding energy in the water cluster associated with the ultrafast ESPT process.

INTRODUCTION

Hydrogen bonding interaction and associated intramolecular processes like proton transfer in biomolecules following photoexcitation is of fundamental importance in modern chemistry and has received significant attention in recent time (1,2). In the past years, the hydrogen bonding effects on the structures and dynamics of many important molecular systems have been well investigated (3–11). For example, Zhao and Han have extensively studied hydrogen bonding in the ground and excited states of organic and biological chromophores as well as its influence to their structures and dynamics in solution by use of combined experimental and theoretical methods. They have demonstrated that intermolecular hydrogen bonds formed between carbonyl chromophores and polar protic solvents can be significantly strengthened in electronically excited states of carbonyl chromophores (11), whereas it gets weakened for thiocarbonyl chromophores (4). Furthermore, they have also reported that radiationless deactivation processes, such as internal conversion (IC), intersystem crossing

(ISC), photoinduced electron transfer (PET), excited state intramolecular proton transfer (ESIPT) and excited state double proton transfer (ESDPT) etc. are strongly influenced by excited state intermolecular hydrogen bonding interactions (5–7). Their study demonstrates that molecular photochemistry (like intramolecular charge transfer [ICT]) in solution can be tuned by hydrogen bonding interactions in electronically excited states (7). Very recently, studies involving site-specific solvation (SSS) of the photoexcited protochlorophyllide *a* (Pchl id e *a*) in methanol using the time-dependent density functional theory method, have theoretically confirmed that intermolecular coordination and hydrogen bonds between Pchl id e *a* and methanol molecules can be strengthened in the electronically excited state of Pchl id e *a* (3). Moreover, the SSS of the photoexcited Pchl id e *a* in methanol can be induced by the intermolecular coordination and hydrogen-bond strengthening upon photoexcitation. Although studies mentioned above have well investigated the various aspects of excited state hydrogen bonding interactions, less is known about excited state proton transfer (ESPT) in organic molecules and essentially their interaction with solvent molecules. Importantly, ESPT is a fundamentally important process that plays a crucial role in many chemical and biological processes. To study the hydrogen bonding interactions and their consequence in the proton transfer, various organic photoacids are found to be ideal model systems, where a significant reduction of pK_a of the organic molecules upon photoexcitation allows measurement of ESPT process conveniently. Over the past few decades, various photoacids have been extensively studied in different solvents as well as in nanoscopic confined environments (12–14). In the present study, we have used a model ESPT probe 1-naphthol (NpOH) in a binary mixture of water and dioxane (DX).

NpOH is a weak base in the ground state ($pK_a = 9.5$). However, in the first excited electronic state, the pK_a^* of NpOH in aqueous solution is about 0.5 (15). The fluorescence of the NpOH molecule lies in the near UV, and in many solvents it is more highly structured than that of the conjugate base, 1-napholate anion (NpO $^-$), which lies in the blue, and is always broad and featureless (16). The acid–base behavior of NpOH has been studied in liquid solutions (16,17) and supersonic jets (18,19). It has been shown that the ESPT of NpOH requires adequate solvation for the stabilization of the polar transition state and the photoproducts (NpO $^-$ and H $^+$). It is observed that with strong gas-phase bases (ammonia, piperidine and triethylamine) proton transfer from NpOH occurs in small

*Corresponding author email: skpal@bose.res.in (Samir Kumar Pal)
© 2012 Wiley Periodicals, Inc.
Photochemistry and Photobiology © 2012 The American Society of Photobiology 0031-8655/12

clusters (number of water molecules, $n < 4$), with a step-like dependence on cluster size (20). However, for weaker gas-phase bases such as H_2O , no proton transfer has been detected up to water cluster sizes of $n \approx 10$ and the ESPT process appears in the larger water clusters of $n \geq 30$ (19,21). The proton transfer rate is believed to be controlled by the rate at which water relaxes (solvation) around the NpOH , *via* interaction with two electronic excited states namely 1L_b and 1L_a (the axes b and a refer to the long and short axes of the aromatic ring, respectively) (19). However, studies focusing on the solvent dynamics around photoacids are sparse in the present literature. This is due to the presence of two competing relaxation processes (intermolecular proton transfer and solvation stabilization) in the excited state, which is quite complicated to interpret separately. Earlier attempts have been made to correlate the effect of solvation dynamics on the proton transfer reaction. In one of the studies, Moog and Maroncelli (22) have observed a time-dependent Stokes shift of the normal emission in 7-azaindole in alcohols and clearly revealed that the energy window for the observation of true proton transfer rate without any complication from the dynamics of polar solvation. However, a detail of the dynamics of solvation of an ESPT probe prior to the proton transfer needs attention and is one of the motives of the present study.

The role of water structural reorganization is expected to be evident in the case of organized assemblies, for example, in the nanocavity of cyclodextrin and the surfactant aggregates (micelles and lipids), where water relaxation is much slower compared with bulk water (23,24). It is indeed observed that ESPT process in cyclodextrin (25), micelle (26), and lipids (27,28) is markedly retarded by one to two orders of magnitude compared with that in bulk water. These results largely suggest that the solvents affect ESPT of NpOH in a number of ways. For example, the nature and cluster size of proton acceptor solvent molecules has a great influence on ESPT (19). Apart from this, the dynamical participation of water in the ESPT process is expected to be retarded by relaxation processes in the solvent shells around the solute (here NpOH). Despite the several advantages in the conventional organized assemblies (micelle, reverse micelle or cyclodextrin cavity), the properties of water in micelles or cyclodextrin cavities depend on their charge and hydrophobic/hydrophilic character, as well as structure of the surfactant head group and length of the hydrophobic tail (29,30). Thus, they form hydrogen bond structure with water molecules to different extent. While binary mixture composed of hydrophilic and hydrophobic solvent are devoid of any such complicacy. In this regard, DX has a unique property to form small water clusters where the dynamical properties of the water molecules can be monitored by changing the composition of the mixture (31). Moreover, DX has a distinctive property to solubilize water in all proportions in spite of its negligible polarity and it also offers a substantial number of noninteracting hydrophobic sites ($-\text{C}_2\text{H}_4$ segments) to water. In addition, DX can form a hydrogen bond with water, but cannot self-associate to form clusters. As the water content increases the water cluster size grows and a local concentration of water molecules increases. In a recent study from our group (31), we have explored the nature of solvation dynamics and hydrogen bonding in the nanocluster of water in DX environments. Thus, such a system provides a rare opportunity for

studying the role of solvation dynamics on ESPT process, which is slower, compared with that of bulk water. In addition, the H-bonded structure of water in such nanoscopic environments mimic the isolated water molecules in biological systems like lipid bilayer, protein interior etc. where proton transfer processes are known to occur.

In the present study, we study the role of solvation dynamics on the ESPT process of NpOH in water–DX nanoclusters. The dynamics of proton transfer and solvent relaxation have been examined through picosecond-resolved fluorescence measurements. To ascertain the types of species present in the water–DX mixture, we have used picosecond-resolved area normalized emission spectroscopy (TRANES). The time-resolved fluorescence Stokes shift method has been adopted to study the solvation dynamics of water in the nanoclusters. To compare the solvent relaxation dynamics as revealed by the probe NpOH , we have measured the solvation dynamics of water with another well-known solvation probe Coumarin 500 (C500). To understand the energetics of the hydrogen bonded network in hydrophilic (water)-hydrophobic (DX) mixture, we have studied the excited state kinetics of both the probes at different temperatures. Similarity in both results reveals the importance of hydrogen bonding interaction in the solvent relaxation process and thereby provides a strengthened connection between solvation dynamics and ESPT process.

MATERIALS AND METHODS

1-Naphthol was purchased from Sigma–Aldrich. Coumarin 500 (C500) was a product of Exciton. 1,4-DX was purchased from Spectrachem and was of highest purity available and used without further purification. Double-distilled water was used for preparation of water–DX mixture of different concentrations. Absorption and emission spectra were recorded with a Shimadzu UV-2450 spectrophotometer and a JobinYvon Fluoromax-3 fluorimeter, respectively. We used a commercially available picosecond diode laser-pumped (LifeSpec-ps) time-resolved fluorescence spectrophotometer from Edinburgh Instruments (Livingston) for time-resolved measurements. For 409 nm excitation (for electronic excitation of C500), a picoquant diode laser was used with instrument response function (IRF) of 80 ps. For NpOH , we have used a femtosecond-coupled TCSPC (time-correlated single-photon counting) setup in which the sample was excited by the third harmonic laser beam (290 nm) of the 870 nm (0.5 nJ per pulse) using a mode-locked Ti-sapphire laser with an 80 MHz repetition rate (Tsunami, Spectra-Physics), pumped by a 10 W Millennia (Spectra-Physics) followed by a pulse-peaker (rate 8 MHz) and a third harmonic generator (model 3980, Spectra-Physics). The third harmonic beam was used for excitation of the sample inside the TCSPC instrument (IRF = 70 ps) and the second harmonic beam was collected for the start pulse. Luminescence transients were fitted by a commercially available software F900 (LifeSpec-ps) from Edinburgh Instruments using a nonlinear least squares fitting procedure to a function ($X(t) = \int_0^t E(t')R(t-t')dt'$) comprising of convolution of the IRF ($E(t)$) with a sum of exponentials ($R(t) = A + \sum_{i=1}^N B_i e^{-t/\tau_i}$) with pre-exponential factors (B_i), characteristic lifetimes (τ_i) and a background (A). Relative concentration in a multiexponential decay was finally expressed as; $a_n = (B_n / \sum_{i=1}^N B_i) \times 100$.

The time-dependent fluorescence Stokes shifts, as estimated from time-resolved emission spectroscopy (TRES; 32,33), were used to construct the normalized spectral shift correlation function or the solvent correlation function $C(t)$ defined as

$$C(t) = \frac{v(t) - v(\infty)}{v(0) - v(\infty)} \quad (1)$$

where $v(0)$, $v(t)$ and $v(\infty)$ are the emission maximum (in cm^{-1}) at time zero, t and infinity, respectively. The $v(\infty)$ values had been taken to be

the emission frequency beyond which an insignificant or no spectral shift was observed. The $C(t)$ function represents the temporal response of the solvent relaxation process, as occurs around the probe following its photoexcitation and the associated change in the dipole moment. To ascertain the types of species present in the water–DX mixture, we adopted the time-resolved area normalized emission spectra (TRANES) technique developed by Periasamy's group (34). TRANES is a model free modified version of TRES mentioned earlier. A useful feature of the method is that an isoemissive point in the spectra involves two emitting species (could be same molecule in different environments), which are kinetically coupled either irreversibly or reversibly or not coupled at all.

RESULTS AND DISCUSSION

The absorption and emission spectra of NpOH in pure water, DX and water–DX mixtures are shown in Fig. 1. Dynamic light scattering (DLS) studies confirm the formation of water nanocluster (1–400 nm) in the water–DX mixtures. The absorption spectra are insensitive to the relative concentrations of water and DX solvent mixture. This suggests that the ground state property of NpOH hardly depends on the polarity of the host solvent. However, the emission spectra (Fig. 1b) show two distinct emission bands whose intensities are sensitive to water concentrations. In a pure DX solvent, there is a single emission band centered at 360 nm. On addition of water, the intensity of this band decreases, and a new band grows at 460 nm. The short wavelength emission has

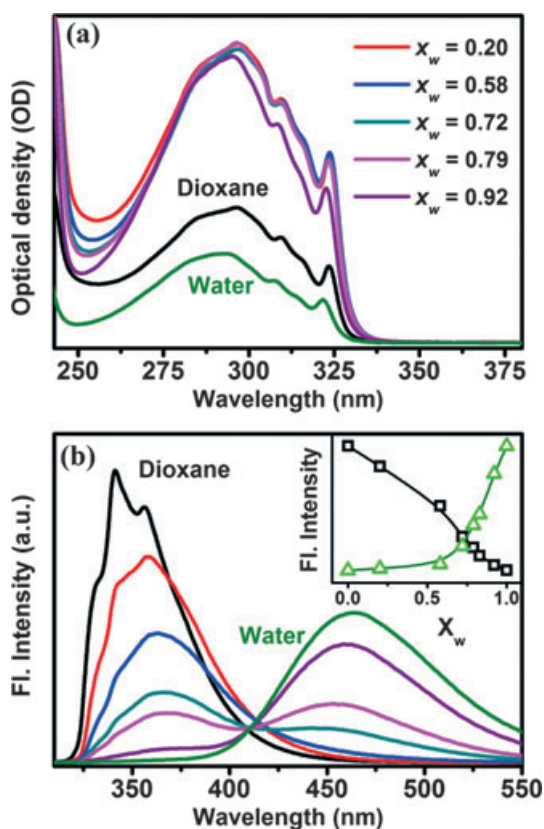
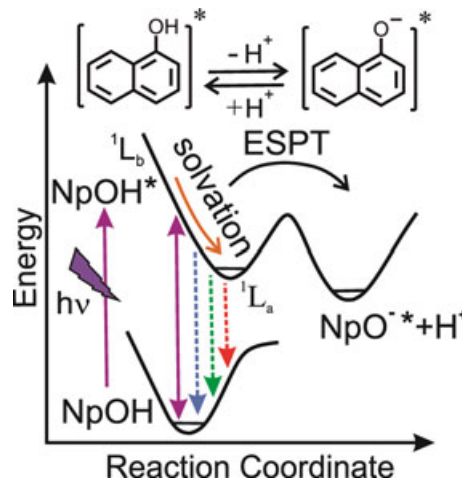


Figure 1. (a) Absorption and (b) emission spectra of 1-naphthol in water–DX mixture with different mole fraction (x_w) of water. Inset: plot of variation of the normalized-fluorescence intensity of the protonated naphthol (NpOH) and deprotonated (NpO⁻) forms at different mole fractions of water in water–DX mixture.

been attributed to protonated NpOH, whereas the long-wavelength emission to the deprotonated 1-naphtholate anion (NpO⁻) characteristic of the ESPT between NpOH and water solvent (35). The relative fluorescence intensity of the protonated and deprotonated form with increasing mole fractions of water is shown in the inset of Fig. 1b. As the water content increases, the ESPT process is more and more facilitated. This progressive increase in ESPT is related to polarity of the solvent mixture, which mainly refers to the hydrogen bonding ability of the solvent. One may note that the ESPT process is believed to follow a three-state two-step model (19) as shown in Scheme 1. Optical excitation of NpOH leads to ¹L_b state. Depending upon the hydrogen bonding ability and dielectric constant, the relatively nonpolar first excited state relaxes to the second polar acidic excited state ¹L_a that has the oxygen-to-ring charge transfer character, which is required for ESPT. This is followed by removal of the proton in coordination with relaxation of the solvent around the new ion pair. Thus, properties of the solvent and relaxation dynamics determine whether only the first or both steps take place.

In pure nonpolar DX, the only emitting species is first relatively nonpolar excited state and as such there is no ESPT. However, in the case of water–DX mixture, after the first step, the lowest excited state interacts with the solvent water molecule, leading to the ESPT reaction. It should also be noted that there is no sign of ESPT reaction up to $x_w = 0.58$ (Fig. 1b). This might be due to NpOH that does not get enough water molecules in their immediate environment. Previously, it was shown that clusters composed of a minimum of approximately 30 or more water molecules are required around the probe NpOH so that proton affinity of the cluster is sufficient to promote ESPT (19). The observed decrease in the fluorescence intensity at *ca* 330 nm (characteristic of neutral NpOH) and consecutive growth at *ca* 450 nm (characteristic of NpO⁻) are the consequences of the progressive increase in water cluster size (Fig. 1b). It has to be noted that at 0.79 mole fraction of water (x_w), the intensity of the protonated and deprotonated forms are comparable (Fig. 1b).



Scheme 1. Schematic illustration of the excited state solvation of 1-naphthol in coordination with proton transfer process. Optical excitation of NpOH leads to ¹L_b state, which attains the second polar acidic excited state ¹L_a after solvation and finally removal of the proton to the surrounding water molecules.

Hence, the time-resolved measurements are carried out at this particular concentration ($x_w = 0.79$). The choice of this concentration also lies in the fact that at $x_w = 0.79$, the water clusters have different geometry than that in the bulk water due to the breakage of the hydrogen bond network. Pure water clusters begin to appear at the critical point $x_w \geq 0.83$ (36). This is also reflected in the faster relaxation rate with increase in the water content in water–DX, which increases the number of hydrogen bonds per oxygen atom (31). Our DLS experiment confirms a cluster size of ~ 350 nm in the x_w of 0.79 (data not shown).

We have measured fluorescence decays at a number of wavelengths across the emission spectrum of NpOH in water–DX mixture of $x_w = 0.79$ and the fitting parameters are tabulated in Table 1. Figure 2a shows the decay transients at three representative wavelengths (330, 440 and 490 nm). It is observed that the fluorescence decays are wavelength dependent, and there is evidence of a rise in the intensity as a function of time at the longest wavelengths (490 nm). It is known that this type of rise in intensity is characteristic of an excited state process in which the emitting species is not directly excited but rather forms, from a previously excited state (33). We have used the fluorescence transients to construct TRES (time-resolved emission spectra) as shown in Fig. 2b. In TRES, the temporal profiles are well fitted by the sum of two lognormal functions revealing two excited state processes.

At time $t = 0$ ns, only one peak centered at $27\,140\text{ cm}^{-1}$ is observed revealing the signature of neutral NpOH. As time progresses, the peak intensity decreases (Fig. 2b) and shows time-dependent Stokes shift (TDSS), which is indicative of dynamic solvation. A new band near $22\,332\text{ cm}^{-1}$ appears, which is a characteristic of ESPT. The intensity of this new band keeps growing, which can be readily used to measure the kinetics of the NpO^- ion formation. Thus, the rate of proton transfer (formation of NpO^-) is estimated by plotting the time-dependent intensity at $22\,332\text{ cm}^{-1}$ as shown in the inset of Fig. 2b, which reveals a time constant of 220 ps (Table 2).

From the TRES it is also evident that emission from locally excited state (LE) is dominant in the wavelength region of $30\,303\text{--}23\,809\text{ cm}^{-1}$. On the other hand, the emission from the NpO^- is prevailing in the region of $21\,739\text{ cm}^{-1}$. It is evident from Table 1 that the longer time component (*ca* 2.3 ns) of the fluorescence transients gradually increases with the increase in the detection wavelength (from 2.4 ns at 330 nm to 8.0 ns at 450 nm) of LE emission. The observation is consistent with the fact that NpOH molecules, which are stabilized by the solvation, are expected to encounter higher solvation energy barrier for the ESPT process as shown in Scheme 1. Our observation is consistent with the results reported in the earlier femtosecond-resolved studies on a twisted ICT probe (2-(*p*-toluidino)naphthalene-6-sulfonate; TNS), where two competing processes, namely solvation and twisting dynamics, were

Table 1. The fluorescence lifetimes for 1-naphthol and Coumarin 500 in water–dioxane mixture with $x_w = 0.79$ with a standard error of *ca* 10%.

	Wavelength (nm)	a_1 (%)	τ_1 (ps)	a_2 (%)	τ_2 (ps)	a_3 (%)	τ_3 (ps)
1-Naphthol	330	10	220	82	1000	8	2350
	340	3	260	86	970	11	2140
	350	–	–	95	1010	5	2750
	360	–	–	95	1010	5	2640
	370	–12	20	105	980	7	2760
	380	–12	70	108	1020	4	2860
	390	–18	90	113	1020	5	3400
	400	–16	50	111	1060	5	5840
	410	–12	70	102	1070	10	6710
	420	–25	80	102	1150	23	7450
	430	–35	100	90	1300	45	7580
	440	–45	160	72	1560	73	7780
	450	–69	220	61	1930	108	8020
	460	–93	270	67	3110	126	8320
	470	–120	360	77	3530	143	8550
	480	–154	380	100	4130	154	8830
490	–179	430	167	5080	112	10 260	
C500	450	70	60	5	560	25	4980
	460	55	70	5	1050	040	5010
	470	43	80	5	1380	52	5000
	480	28	100	8	2410	64	5070
	490	18	100	10	2630	72	5060
	500	11	100	15	2960	74	5120
	510	3	110	32	3640	65	5310
	520	1	100	27	3600	73	5200
	530	–3	420	9	2110	94	4950
	540	–10	700	11	1180	99	4880
	550	–14	540	13	1000	101	4880
	560	–7	240	12	3040	95	4980
	570	–8	200	56	4120	52	5480
	580	–11	170	52	4140	59	5370
	590	–19	70	83	4420	39	5270
	600	–36	80	11	3800	125	4875

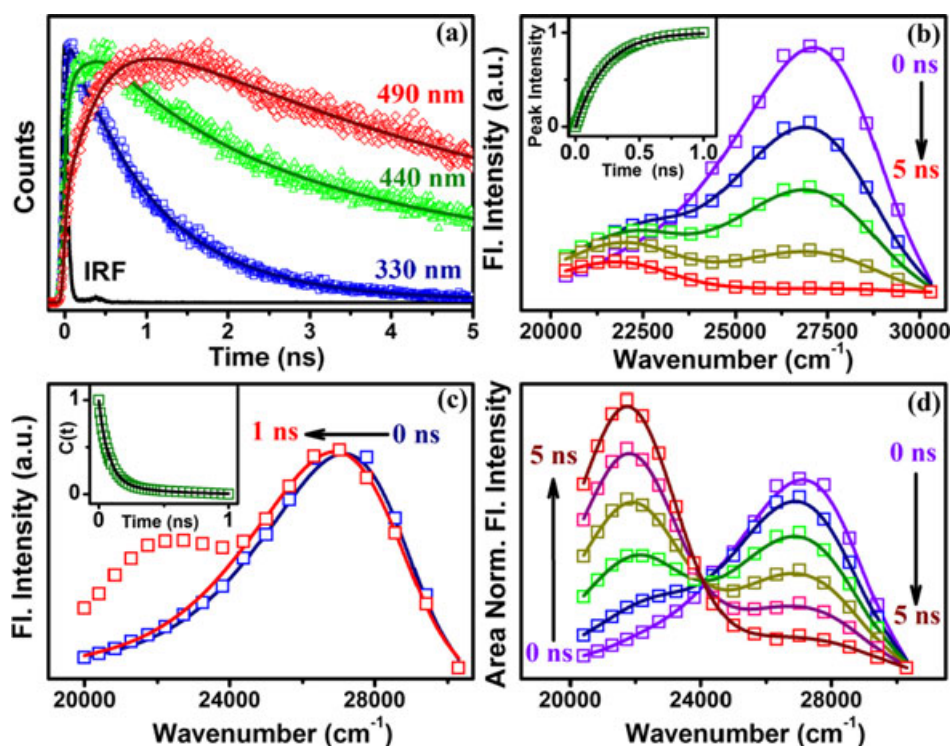


Figure 2. (a) Picosecond-resolved decay transients of 1-naphthol at 330, 440 and 490 nm in water–DX mixture with $x_w = 0.79$ at room temperature (excitation at 300 nm). (b) Time-resolved emission spectra (TRES) of 1-naphthol for $x_w = 0.79$ in water–DX mixture. The peak fluorescence intensity at 450 nm of naphtholate anion (NpO^-) is shown in the inset. (c) Normalized time-resolved emission spectra of 1-naphthol in water–DX mixture with $x_w = 0.79$. The corresponding solvent correlation function, $C(t)$, has been shown in the inset. (d) TRANES of 1-naphthol for $x_w = 0.79$.

Table 2. Proton transfer and solvent correlation time constants for 1-naphthol and Coumarin 500 in water–dioxane mixture with $x_w = 0.79$ with a standard error of *ca* 10%.

Probe	Temperature (K)	τ_1/ps (%)	τ_2/ps (%)	$\langle \tau \rangle$ (ps)	τ_{PT} (ps)
1-Naphthol	278	76 (90)	1000 (10)	168	380
	293	70 (85)	340 (15)	110	220
	313	65 (100)	–	65	230
Coumarin 500	278	99 (87)	55 (13)	160	–
	293	67 (55)	15 (45)	105	–
	313	72 (69)	13 (31)	89	–

found to be major deactivation channels in the excited state of the probe molecule (37).

To show the TDSS of LE NpOH more clearly, we have normalized the fluorescence intensity at $27\,140\text{ cm}^{-1}$ and fitted with a lognormal function as shown in Fig. 2c. The observed Stokes shift is roughly 255 cm^{-1} over a time window of 1 ns. From the dynamic Stokes shift, we have constructed the solvent correlation function ($C(t)$) to obtain the solvation time constants (inset of Fig. 2c). The constructed $C(t)$, can be fitted biexponentially with time constants of 70 (85%) and 340 ps (15%) (Table 2). It should be noted that both the observed time constants are much slower than the subpicosecond solvation time constant of bulk water (38). These slow components might have their genesis in the translational diffusion of water into the solvation shell displacing the nonpolar solvent molecule in the

cluster (39–41). Such slow solvation dynamics in relatively concentrated solutions of polar fluid in hydrophobic solvents has previously been reported (39,42). The average solvation time constant ($a_1\tau_1 + a_2\tau_2 = \langle \tau_s \rangle = 110\text{ ps}$) in our case is in good agreement with that reported by Mitra *et al.* (31) with Coumarin 500 for a similar system with $x_w = 0.826$. A significant retardation in the proton transfer rate and the dynamics of solvation in our experimental condition ($x_w = 0.79$) can be rationalized as follows.

In pure water, NpOH undergoes ESPT in *ca* 35 ps, causing a 35 ps fall time of the protonated species and a *ca* 35 ps rise time for the deprotonated product, 1-naphtholate anion (35). At $x_w = 0.79$, we have also observed a fall (at 330 nm for the protonated form) and rise (at 450 nm for the deprotonated form) time of *ca* 220 ps (Table 1). Thus, the ESPT in water–DX mixture is slowed down approximately seven times compared with that in pure water. The reduction in ESPT has two probable causes. First, local concentration of water molecules near the photoacid, NpOH in water–DX mixture should be sufficient to promote proton transfer. In fact, a cluster composed of minimum of 30–50 water molecules is required to promote ESPT (20). Second, the solvation reorganization in water–DX mixture (*ca* 110 ps) is much slower compared with that in bulk water (*ca* 1 ps). For water–DX mixture, water clusters are present with considerably different geometry than that in the pure water due to breakage of the hydrogen bond network. Previously, Knochenmuss and Smith suggested that the ESPT rate is controlled by the rate at which the water relaxes around the NpOH fluorophore, *via* interaction

with two electronic excited states (43). Thus, time-resolved analysis as discussed above clearly indicates that the dynamical rearrangement (solvation of average time of 110 ps) is an essential requirement prior to the ESPT (average time of 220 ps). An isoemissive point at $24\,086\text{ cm}^{-1}$ in the TRANES as shown in Fig. 2d indicates the presence of two distinct species (34) namely neutral NpOH and the NpO^- anion revealing characteristic peaks at $27\,140$ and $22\,332\text{ cm}^{-1}$. It is evident from Fig. 2d that at time $t = 0$, there is only one emission band centered at $27\,140\text{ cm}^{-1}$ and the emission is from the LE NpOH. As time progresses, the band at $22\,332\text{ cm}^{-1}$ is clearly seen to grow at the expense of the one at $27\,140\text{ cm}^{-1}$.

To check the reliability of the solvation time constants as revealed by NpOH, we have studied the excited state dynamics

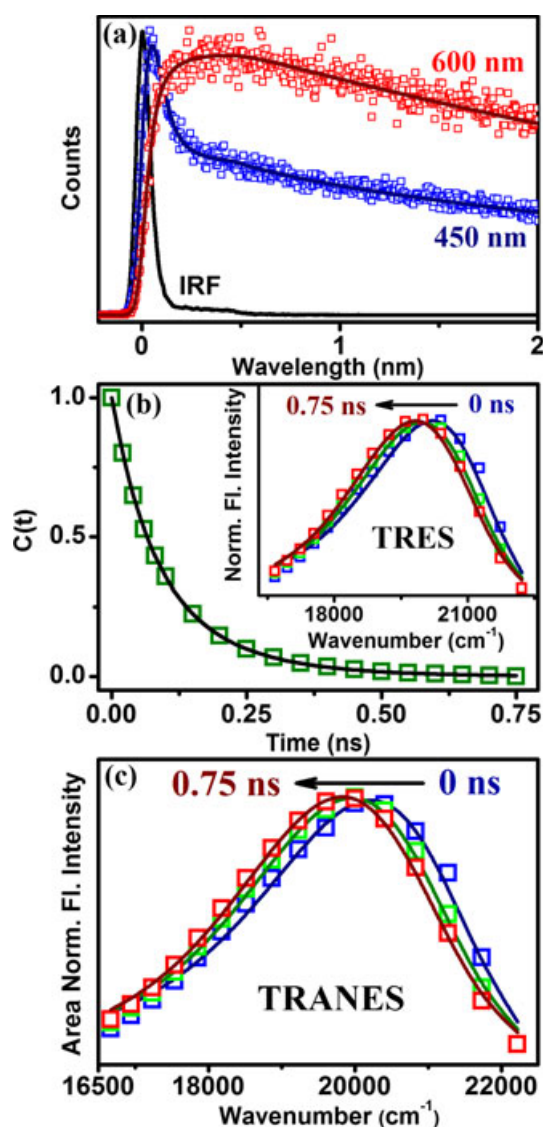


Figure 3. (a) Picosecond-resolved decay transients of C500 at 450 and 600 nm detection wavelength in water-DX mixture with $x_w = 0.79$ ($\lambda_{\text{ex}} = 409\text{ nm}$). (b) Solvent correlation function, $C(t)$, of C500 in water-DX mixture with $x_w = 0.79$. The corresponding TRES has been shown in the inset. (c) TRANES of C500 in water-DX mixture with $x_w = 0.79$.

of Coumarin 500 (C500), a well-known solvation probe in the same composition of water-DX mixture. To construct the TRES, the decay transients of C500 have been monitored at 16 different wavelengths from 450 to 600 nm with 10 nm interval. Figure 3a represents the emission decays at two extreme wavelengths (450 and 600 nm). On the blue edge of the spectrum (450 nm), the fluorescence transient undergoes decay, whereas on the red edge (600 nm) it rises, which is the clear indication of relaxation dynamics of C500. The inset of Fig. 3b denotes the constructed TRES of the system. The constructed TRES shows a spectral shift of 395 cm^{-1} and the corresponding solvent response function (Fig. 3b) is well fitted biexponentially with time constants of 67 ps (55%) and 150 ps (45%; Table 2). It is to be noted that TRANES analysis of C500 (Fig. 3c) is devoid of any isoemissive point indicating the fact that there is a single emitting species in the excited state and the continuous time evolution is due to the solvation dynamics only. The average solvation time constant of 105 ps is in good agreement with that obtained using NpOH (Table 2).

The solvent reorganization around NpOH certainly involves breaking of hydrogen bonds as molecules translate and rotate, and this will require activation. It is therefore constructive to perform a temperature dependent study of the system. Figure 4 shows the emission spectra of NpOH and C500 with $x_w = 0.79$ at five different temperatures. From Fig. 4a it is evident that emission intensity of NpOH decreases significantly with increasing temperature. In fact, the extent of decrease of fluorescence intensity for the anionic form

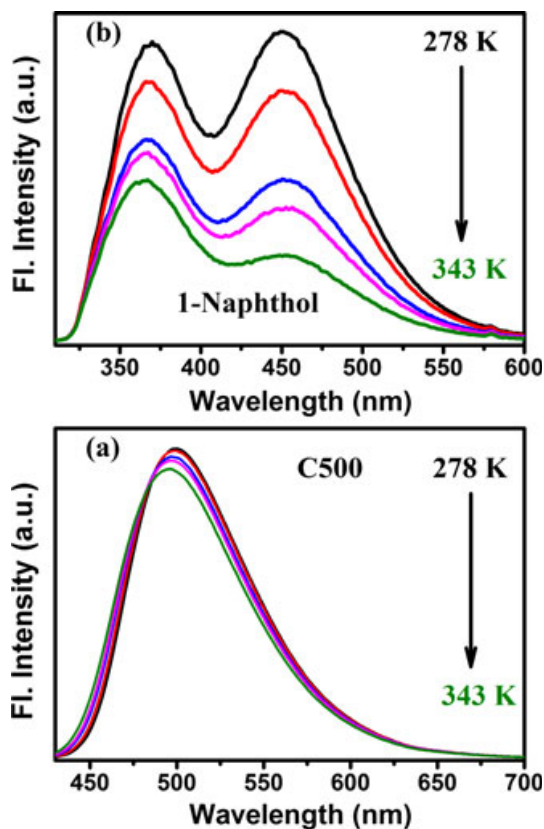


Figure 4. Emission spectra of 1-naphthol (a) and C500 (b) in water-DX mixture of $x_w = 0.79$ at different temperatures.

(450 nm) is higher than that for the neutral species (360 nm). A small blueshift (around 4-5 nm) of the peak at 360 nm is also evident. However, no such change in the absorbance spectra is found for NpOH with increasing temperature (data not shown). The steady-state emission spectra of the system using C500 (Fig. 4b) shows a marginal (3-4 nm) blueshift as the temperature is increased from 278 to 343 K. The observed blueshift indicates a less polar environment experienced by the probe at elevated temperatures. To gain more insight, we performed time-resolved measurement of $x_w = 0.79$ at five different temperatures. The constructed TRES are shown in the Fig. 5a,b at 278 and 313 K, respectively. TDSS of the protonated species is used to construct solvent correlation function and the values are listed in Table 2. The overall decrease of the average solvation time on increasing temperature reveals that an increase in temperature accelerates the

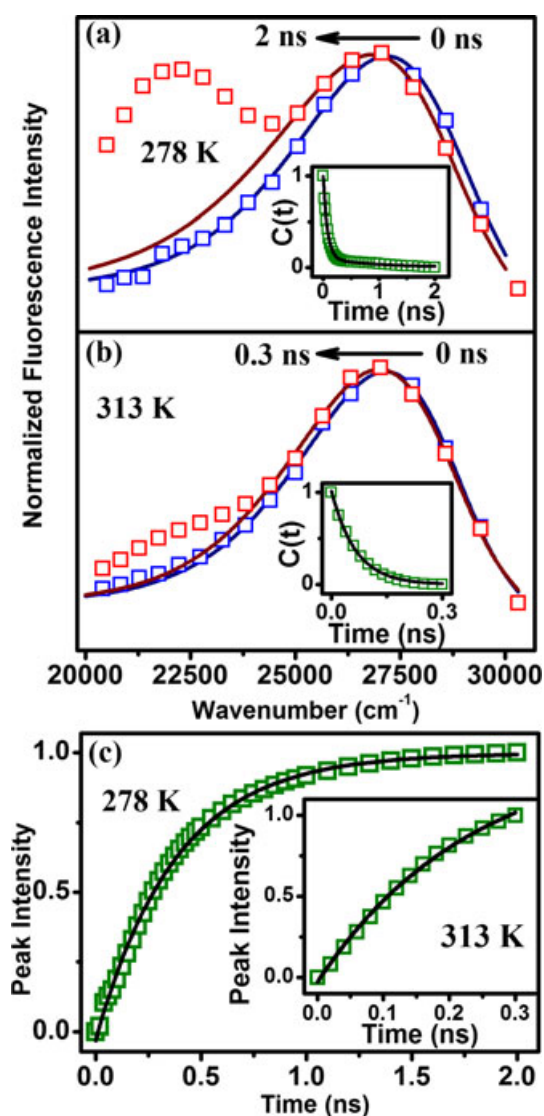


Figure 5. Normalized time-resolved emission spectra of 1-naphthol in water-DX mixture with $x_w = 0.79$ at 278 K (a) and 313 K (b). The corresponding solvent correlation function, $C(t)$, has been shown in the inset. (c) The increase in peak intensity of the deprotonated form (NpO⁻) at two different temperatures (278 and 313 K), respectively.

solvation process. It has to be noted that due to our limited instrumental resolution we could not resolve the water dynamics at higher temperature (>313 K) in the present system. The temperature-induced acceleration of solvation dynamics is possibly due to breakdown of the hydrogen bond network followed by the formation of smaller clusters with increasing temperature (31). In fact, it has been suggested that DX specifically binds five or six water molecules into more strongly bound hydrogen-bonded structures than in liquid water itself (44,45). There exists a dynamic equilibrium between the bound type (strongly hydrogen bonded to ether oxygen of DX) and free type (not directly hydrogen bonded to DX). The energetic of the exchange depends upon the strength and the number of hydrogen bonds among the water molecules at the interface (*i.e.* water-DX interface). The bound to free type transition of water molecules with temperature is assumed to be governed by an Arrhenius type of activation energy barrier crossing model (46,47). We fit an Arrhenius plot using the $\langle \tau_s \rangle$ values listed in Table 2 (Fig. 6a). Plots of $\ln(1/\langle \tau_s \rangle)$ vs $1/T$ produce good linear fit with corresponding activation energy (E_{act}) values of 4.60 ± 0.2 kcal mol⁻¹. We also perform similar measurement (Fig. 6b) using C500 in identical system, which purely senses solvent relaxation (Table 2) and E_{act} is found to be 2.85 ± 0.4 kcal mol⁻¹. Solvent reorganization results from solvent relaxation around the solute molecule (fluorophore) following a change in the excited state dipole moment. The difference in the activation

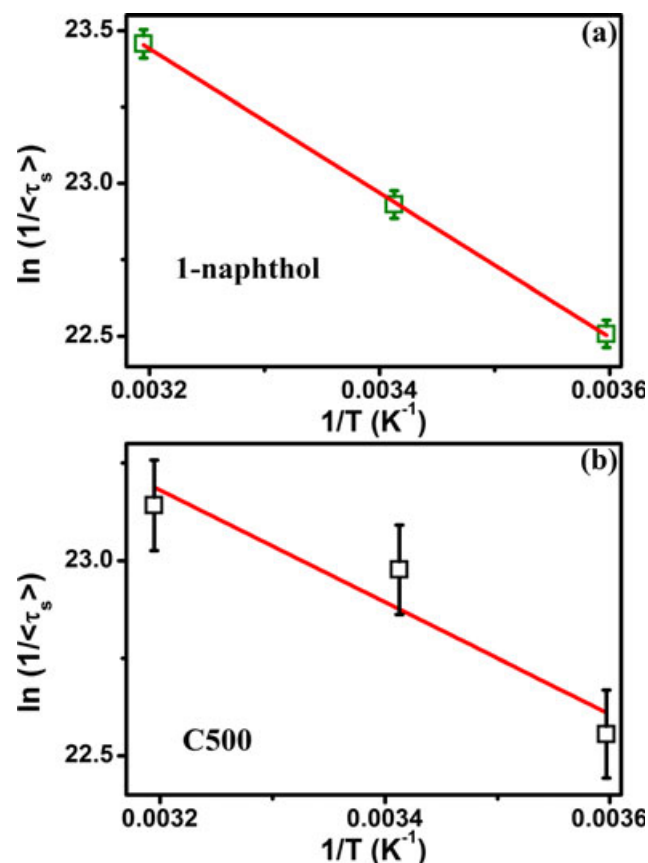


Figure 6. Arrhenius plot for water-DX mixture in $x_w = 0.79$ with two different dyes (1-naphthol and C500). The solid lines are the best linear fit. The error bars are of 0.2% and 0.5%, respectively.

energies is probably due to the difference in specific hydrogen bonding interactions of the probe fluorophores in the water clusters (31,42).

Having understood the temperature-induced acceleration of solvation dynamics, we now focus on the proton transfer rate. The peak intensity of the deprotonated form provides the value of proton transfer time constant. The proton transfer time constant becomes faster on raising the temperature from 278 to 293 K and then does not change appreciably (Table 2). This is in contrast to the solvation dynamics where a progressive decrease in average solvation time constant is observed with increasing temperature. This discrepancy can be understood as follows. As discussed earlier, ESPT is mainly controlled by two factors namely local concentration of water molecules near the photoacid and solvent reorganization. We have discussed that at elevated temperatures, the hydrogen bond network of clusters break down and isolated small clusters consisting of different geometry of hydrogen bonded water start growing. This lowers the polarity of the system due to breakage of hydrogen bonded network, which is also evident from the steady-state emission spectra of the probe as discussed earlier (Fig. 4a,b). Both the lowering in the polarity and local concentration of water favor the emission from the relatively nonpolar first excited state 1L_b and disfavor second polar acidic excited state 1L_a that has the oxygen-to-ring charge transfer character, which is required for ESPT.

CONCLUSION

Our study explores the role of solvent relaxation on ESPT of NpOH in water–DX mixture quantitatively. Time-resolved studies distinctly differentiate the dynamics of two time-dependent excited state processes, the solvent relaxation and the deprotonation. The extent of proton transfer of NpOH is found to be retarded in water–DX mixture compared with that in bulk water. This retardation is attributed to the local concentration of water molecules near the photoacid and solvent reorganization. Solvent dynamics become faster with increasing temperature due to breakage of cooperative hydrogen bond network present in the large clusters to smaller clusters. Increased solvent relaxation at higher temperature makes deprotonation faster. ESPT of a photoacid is an optimization between the local concentration of water and solvent relaxation. At elevated temperature local concentration of water reduces due to breakdown of hydrogen bonded network and ESPT does not change appreciably, although solvation becomes faster.

Acknowledgements—This work was supported by DST, India (SR/SO/BB-15/2007). Surajit Rakshit and Pramod Kumar Verma thank CSIR, India for the fellowships.

REFERENCES

- Lukacs, A., A. Haigney, R. Brust, R.-K. Zhao, A. L. Stelling, I. P. Clark, M. Towrie, G. M. Greetham, S. R. Meech and P. J. Tonge (2011) Photoexcitation of the blue light using FAD photoreceptor AppA results in ultrafast changes to the protein matrix. *J. Am. Chem. Soc.* **133**, 16893–16900.
- Chuang, W.-T., C.-C. Hsieh, C.-H. Lai, C.-H. Lai, C.-W. Shih, K.-Y. Chen, W.-Y. Hung, Y.-H. Hsu and P.-T. Chou (2011) Excited-state intramolecular proton transfer molecules bearing

- o-hydroxy analogues of green fluorescent protein chromophore. *J. Org. Chem.* **76**, 8189–8202.
- Zhao, G.-J. and K.-L. Han (2008) Site-specific solvation of the photoexcited protochlorophyllide *a* in methanol: formation of the hydrogen-bonded intermediate state induced by hydrogen-bond strengthening. *Biophys. J.* **94**, 38–46.
- Zhao, G.-J. and K.-L. Han (2008) Effects of hydrogen bonding on tuning photochemistry: concerted hydrogen-bond strengthening and weakening. *ChemPhysChem* **9**, 1842–1846.
- Zhao, G.-J. and K.-L. Han (2012) Hydrogen bonding in the electronic excited state. *Acc. Chem. Res.* **45**, 404–413.
- Zhao, G.-J., J.-Y. Liu, L.-C. Zhou and K.-L. Han (2007) Site-selective photoinduced electron transfer from alcoholic solvents to the chromophore facilitated by hydrogen bonding: a new fluorescence quenching mechanism. *J. Phys. Chem. B* **111**, 8940–8945.
- Zhao, G.-J., B. H. Northrop, K.-L. Han and P. J. Stang (2010) The effect of intermolecular hydrogen bonding on the fluorescence of a bimetallic platinum complex. *J. Phys. Chem. A* **114**, 9007–9013.
- Arnaut, L. G. and S. J. Formosinho (1993) Excited-state proton transfer reactions I. Fundamentals and intermolecular reactions. *J. Photochem. Photobiol. A Chem.* **75**, 1–20.
- Formosinho, S. J. and L. G. Arnaut (1993) Excited-state proton transfer reactions II. Intramolecular reactions. *J. Photochem. Photobiol. A Chem.* **75**, 21–48.
- Schowen, K. B., H. H. Limbach, G. S. Denisov and R. L. Schowen (2000) Hydrogen bonds and proton transfer in general-catalytic transition-state stabilization in enzyme catalysis. *Biochim. Biophys. Acta Bioenerg.* **1458**, 43–62.
- Zhao, G.-J. and K.-L. Han (2007) Early time hydrogen-bonding dynamics of photoexcited coumarin 102 in hydrogen-donating solvents: theoretical study. *J. Phys. Chem. A* **111**, 2469–2474.
- Itoh, M., T. Adachi and K. Tokumura (1984) Time-resolved fluorescence and absorption spectra and two-step laser excitation fluorescence of the excited-state proton transfer in the methanol solution of 7-hydroxyquinoline. *J. Am. Chem. Soc.* **106**, 850–855.
- Itoh, M., K. Tokumura, Y. Tanimoto, Y. Okada, H. Takeuchi, K. Obi and I. Tanaka (1982) Time-resolved and steady-state fluorescence studies of the excited-state proton transfer in 3-hydroxyflavone and 3-hydroxychromone. *J. Am. Chem. Soc.* **104**, 4146–4150.
- Cohen, B., D. Huppert, K. M. Kyril, M. Solntsev, Y. Tsfadia, E. Nachliel and M. Gutman (2002) Excited state proton transfer in reverse micelles. *J. Am. Chem. Soc.* **124**, 7539–7547.
- Webb, S. P., S. W. Yeh, L. A. Philips, M. A. Tolbert and J. H. Clark (1984) Ultrafast excited-state proton transfer in 1-naphthol. *J. Am. Chem. Soc.* **106**, 7286–7288.
- Webb, S. P., L. A. Philips, S. W. Yeh, L. M. Tolbert and J. H. Clark (1986) Picosecond kinetics of the excited-state, proton-transfer reaction of 1-naphthol in water. *J. Phys. Chem.* **90**, 5154–5164.
- Harris, C. M. and B. K. Selinger (1980) Acid-base properties of 1-naphthol. Proton-induced fluorescence quenching. *J. Phys. Chem.* **84**, 1366–1371.
- Saeki, M., S.-i. Ishiuchi, M. Sakai and M. Fujii (2001) Structure of 1-naphthol/alcohol clusters studied by IR dip spectroscopy and ab initio molecular orbital calculations. *J. Phys. Chem. A* **105**, 10045–10053.
- Knochenmuss, R. and S. Leutwyler (1989) Proton transfer from 1-naphthol to water: small clusters to the bulk. *J. Chem. Phys.* **91**, 1268–1278.
- Kim, S. K., J. J. Breen, D. M. Willberg, L. W. Peng, A. Heikal, J. A. Syage and A. H. Zewail (1995) Solvation ultrafast dynamics of reactions. 8. Acid-base reactions in finite-sized clusters of naphthol in ammonia, water, and piperidine. *J. Phys. Chem.* **99**, 7421–7435.
- Yoshino, R., K. Hashimoto, T. Omi, S.-I. Ishiuchi and M. Fujii (1998) Structure of 1-naphthol–water clusters studied by IR Dip spectroscopy and ab initio molecular orbital calculations. *J. Phys. Chem. A* **102**, 6227–6233.
- Moog, R. S. and M. Maroncelli (1991) 7-Azaindole in alcohols: solvation dynamics and proton transfer. *J. Phys. Chem.* **95**, 10359–10369.
- Bhattacharyya, K. (2003) Solvation dynamics and proton transfer in supramolecular assemblies. *Acc. Chem. Res.* **36**, 95–101.

24. Bhattacharyya, K. and B. Bagchi (2000) Slow dynamics of constrained water in complex geometries. *J. Phys. Chem. A* **104**, 10603–10613.
25. Hansen, J. E., E. Pines and G. R. Fleming (1992) Excited-state proton transfer of protonated 1-aminopyrene complexes with beta-cyclodextrin. *J. Phys. Chem.* **96**, 6904–6910.
26. Mandal, D., S. K. Pal and K. Bhattacharyya (1998) Excited-state proton transfer of 1-naphthol in micelles. *J. Phys. Chem. A* **102**, 9710–9714.
27. Il'ichev, Y. V., A. B. Demyashkevich and M. G. Kuzmin (1991) Protolytic photodissociation of hydroxyaromatic compounds in micelles and lipid bilayer membranes of vesicles. *J. Phys. Chem.* **95**, 3438–3444.
28. Sujatha, J. and A. K. Mishra (1998) Phase transitions in phospholipid vesicles: excited state prototropism of 1-naphthol as a novel probe concept. *Langmuir* **14**, 2256–2262.
29. Verma, P. K., R. Saha, R. K. Mitra and S. K. Pal (2010) Slow water dynamics at the surface of macromolecular assemblies of different morphologies. *Soft Matter* **6**, 5971–5979.
30. Narayanan, S. S., S. S. Sinha, R. Sarkar and S. K. Pal (2008) Validation and divergence of the activation energy barrier crossing transition at AOT/lecithin reverse micellar interface. *J. Phys. Chem. B* **112**, 2859.
31. Mitra, R. K., P. K. Verma and S. K. Pal (2009) Exploration of the dynamical evolution and the associated energetics of water nanoclusters formed in a hydrophobic solvent. *J. Phys. Chem. B* **113**, 4744–4750.
32. Horng, M. L., J. A. Gardecki, A. Papazyan and M. Maroncelli (1995) Subpicosecond measurements of polar solvation dynamics: coumarin 153 revisited. *J. Phys. Chem.* **99**, 17311–17337.
33. Lakowicz, J. R. (1999) *Principles of Fluorescence Spectroscopy*, pp. 237–270. Kluwer Academic/Plenum, New York.
34. Koti, A. S. R., M. M. G. Krishna and N. Periasamy (2001) Time-resolved area-normalized emission spectroscopy (TRANES): a novel method for confirming emission from two excited states. *J. Phys. Chem. A* **105**, 1767–1771.
35. Lee, J., G. W. Robinson, S. P. Webb, L. A. Philips and J. H. Clark (1986) Hydration dynamics of protons from photon initiated acids. *J. Am. Chem. Soc.* **108**, 6538–6542.
36. Mashimo, S., N. Miura, T. Umehara, S. Yagihara and K. Higasi (1992) The structure of water and methanol in *p*-dioxane as determined by microwave dielectric spectroscopy. *J. Chem. Phys.* **96**, 6358–6361.
37. Zhong, D., S. K. Pal and A. H. Zewail (2001) Femtosecond studies of protein-DNA binding and dynamics: histone I. *Chem-PhysChem* **2**, 219–227.
38. Jimenez, R., G. R. Fleming, P. V. Kumar and M. Maroncelli (1994) Femtosecond solvation dynamics of water. *Nature* **369**, 471–473.
39. Molotsky, T. and D. Huppert (2003) Solvation statics and dynamics of coumarin 153 in dioxane-water solvent mixtures. *J. Phys. Chem. A* **107**, 8449–8457.
40. Cichos, F., A. Willert, U. Rempel and C. von Borczyskowski (1997) Solvation dynamics in mixtures of polar and nonpolar solvents. *J. Phys. Chem. A* **101**, 8179–8185.
41. Chandra, A. and B. Bagchi (1991) Molecular theory of solvation and solvation dynamics in a binary dipolar liquid. *J. Chem. Phys.* **94**, 8367–8377.
42. Mukherjee, S., K. Sahu, D. Roy, S. K. Mondal and K. Bhattacharyya (2004) Solvation dynamics of 4-aminophthalimide in dioxane–water mixture. *Chem. Phys. Lett.* **384**, 128–133.
43. Knochenmuss, R. D. and D. E. Smith (1994) Time and internal energy dependent fluorescence spectra of naphthol-water clusters. *J. Chem. Phys.* **101**, 7327–7336.
44. Tourky, A. R., H. A. Rizk and Y. M. Girgis (1961) The dielectric properties of water in dioxane. *J. Phys. Chem.* **65**, 40–42.
45. Goates, J. R. and R. J. Sullivan (1958) Thermodynamic properties of the system water-*p*-dioxane. *J. Phys. Chem.* **62**, 188–190.
46. Nandi, N. and B. Bagchi (1997) Dielectric relaxation of biological water. *J. Phys. Chem. B* **101**, 10954–10961.
47. Verma, P. K., A. Makhil, R. K. Mitra and S. K. Pal (2009) Role of solvation dynamics in the kinetics of solvolysis reactions in microreactors. *Phys. Chem. Chem. Phys.* **11**, 8467–8476.